Research Article Vol. 32, No. 26 / 16 Dec 2024 / Optics Express 47225
Optics EXPRESS

Near-to-far-field transformation scheme utilizing a modified sinc interpolation method for PSTD simulations

JAKE W. LIU AND SNOW H. TSENG*

Graduate Institute of Photonics and Optoelectronics, National Taiwan University, Taipei 10617, Taiwan
**stseng@ntu.edu.tw*

Abstract: We present a near-to-far-field (NTFF) transformation scheme tailored for pseudospectral time-domain (PSTD) simulations. Surface currents on the NTFF boundary are computed using a modified sinc interpolation method, eliminating the need for local averaging required infinite-difference time-domain (FDTD) simulations. Numerical results for dielectric sphere scattering, compared with Mie solutions, demonstrate that the proposed PSTD scheme achieves root-mean-square errors an order of magnitude lower than FDTD for the far-field patterns. The sinc interpolation method exhibits exceptional accuracy, even when applied to coarse grids.

1. Introduction

The analysis of electromagnetic radiation and scattering phenomena plays a pivotal role in various fields. Central to such analyses is the near-to-far-field (NTFF) transformation technique, which enables the extraction of far-field information from near-field distributions. In time-domain simulations, particularly within the framework of the finite-difference time-domain (FDTD) method, numerous NTFF formulations have been developed to accurately capture far-field responses while adhering to the staggered-grid structure inherent to FDTD.

The pioneering works of Umashankar and Taflove in the early 1980s marked the inception of NTFF transformation techniques within the framework of the FDTD method [1,2]. These seminal contributions laid the groundwork for subsequent advancements in the field, sparking a surge of research endeavors aimed at refining and extending the applicability of such transformations. Over the ensuing decades, a plethora of scholarly works have been published, each contributing to the evolution and diversification of NTFF transformation methodologies [3–14]. Traditionally, NTFF transformations in FDTD simulations have predominantly been executed in the frequency domain. This approach entails the conversion of scattered fields into the frequency domain via either discrete Fourier transform (DFT) or fast Fourier transform (FFT) techniques. Luebbers *et al*. [4] and Yee *et al*. [5] stand among the vanguards of this methodology, devising time-domain far-zone transformations that are particularly well-suited for scenarios necessitating time-domain results or a broad spectrum of frequencies. In [7], Ramahi introduced a novel approach to NTFF transformation leveraging Kirchhoff's surface integral representation. Martin, advancing the discussion of the topic, sought a formulation which requires no interpolation for the FDTD calculations [9]. Recently, a new algorithm of the fast calculation of NTFF transformation based on the spherical coordinates splitting is proposed, which does not rely on the conventional sampling scheme [14]. The contributions of these researchers have significantly enriched the FDTD toolkit, empowering practitioners to tackle a diverse array of electromagnetic problems with enhanced efficiency and accuracy.

However, the discussion surrounding NTFF formulations becomes notably sparse when considering simulations based on the pseudospectral time-domain (PSTD) method, which utilizes collocated grids. PSTD simulations offer distinct advantages, particularly in their ability to compute fields using information from the entire computational domain [15–17]. Unlike FDTD,

#546322 https://doi.org/10.1364/OE.546322
Journal © 2024 Received 30 Oct 2024; revised 26 Nov 2024; accepted 28 Nov 2024; published 11 Dec 2024

Optics EXPRESS

which relies on local approximations, PSTD leverages the spectral properties of the field globally. This allows PSTD to adhere to the Nyquist theorem, ensuring accurate field reconstruction even with a coarser grid. When properly utilized, PSTD excels in modeling large-scale problems [18]. In contrast, FDTD requires a much finer grid to maintain the same level of accuracy (normally, 20 points per smallest wavelength in most simulations), making PSTD more efficient in terms of computational resources while achieving higher precision with fewer grid points. In recent years, there has been notable progress in the application of PSTD techniques to scattering problems, as highlighted in Refs. [18–24], and the NTFF transformation stands out as a crucial step in obtaining the simulation results in the above-mentioned research. Despite this, there remains a gap in the literature regarding the adaptation of NTFF transformations to suit the unique characteristics of PSTD simulations.

In this paper, we address this gap by presenting a novel NTFF transformation scheme tailored specifically for PSTD simulations. Leveraging the inherent capabilities of PSTD in calculating fields, which encompass the entire computation domain, our approach eliminates the need for local averaging processes required by traditional FDTD-based NTFF formulations. Through detailed analysis and simulation results, we demonstrate the effectiveness and accuracy of our proposed scheme in calculating far-field information from PSTD simulations.

2. NTFF transformation

In this section, our focus lies in utilizing the calculated near fields to ascertain the harmonic far fields at specific frequencies. We embark on this exploration by initially elucidating the foundational principles of NTFF transformation, delineating its fundamental concepts and methods. Subsequently, we delve into the existing implementations for FDTD simulations, providing a comprehensive overview of the prevalent techniques employed within this domain.

Having established a solid understanding of the theoretical underpinnings of NTFF transformation within the context of FDTD simulations, we pivot towards introducing a novel NTFF transformation scheme specifically tailored for PSTD simulations. This proposed scheme represents an innovative approach aimed at leveraging the unique computational framework of collocated PSTD to enhance the accuracy and efficiency of NTFF transformations, and a brief discussion on the extension to staggered PSTD is also provided. Through a meticulous examination of the proposed method, we aim to elucidate its intricacies and highlight its potential benefits in the realm of electromagnetic simulation and analysis. In this paper, a three-dimensional (3D) formulation is considered.

2.1. Surface equivalence theorem

As illustrated in Fig. 1, based on surface equivalence theorem [25], the core idea of calculating the far-field from a time-domain simulation is to set a fictitious surface which encloses the scatterers and sources, and then transform the problem under investigation to an equivalence problem in which the fields outside the surface remain the same but the fields inside the surface are zero. To comply with the boundary conditions, the equivalent surface currents on the surface are given by

$$\mathbf{J}_s = \hat{\mathbf{n}} \times \mathbf{H} \tag{1.a}$$

$$\mathbf{M}_s = -\hat{\mathbf{n}} \times \mathbf{E} \tag{1.b}$$

where $\hat{\mathrm{n}}$ is the normal unit vector pointing out of the surface. From the equivalence surface currents given above, a set of vectors can be computed by integrating the surface currents over

Optics EXPRESS

the closed surface to find the far-field radiation

$$\mathbf{N} = \oint_S \mathbf{J}_s e^{ikr' \cos\delta} ds' \tag{2.a}$$

$$\mathbf{L} = \oint_S \mathbf{M}_s e^{ikr' \cos\delta} ds' \tag{2.b}$$

where δ represents the angle between the position of the source point $r'\hat{\mathbf{r}}'$ and the observation point $r\hat{\mathbf{r}}$. $k = 2\pi/\lambda$ is the wave number. The electric far field in spherical coordinate is given by

$$\mathbf{E} = \frac{ike^{ikr}}{4\pi r}[(-L_\phi - \eta_0 N_\theta)\hat{\boldsymbol{\theta}} + (L_\theta - \eta_0 N_\phi)\hat{\boldsymbol{\phi}}] \tag{3}$$

where η_0 denotes the intrinsic impedance of free space. In practice, the NTFF surface in an FDTD simulation is a rectangular box composed of six surfaces on which the equivalent surface currents are easily computed by the calculated electric and magnetic fields following (1). However, the staggered-grid nature of FDTD gives rise to the problematic while choosing such closed surface when both the fictitious electric and magnetic currents are to be aligned on the same surface.

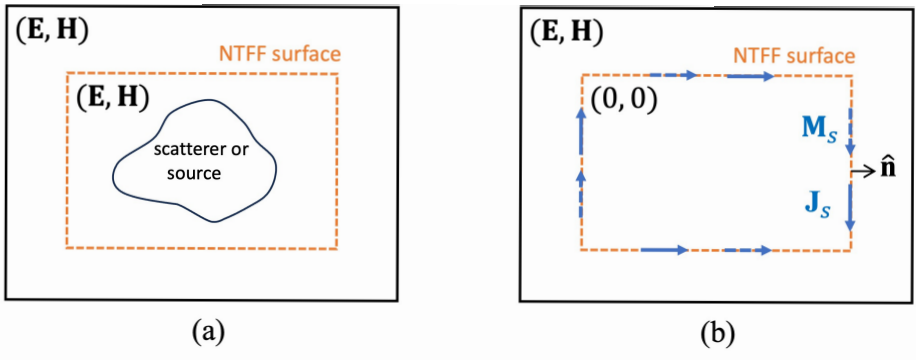

Fig. 1. Illustration of the equivalence theorem as applied to NTFF transformation. The left panel (a) depicts the NTFF surface enclosing the scatterer or source, where the electromagnetic fields are computed directly. The right panel (b) shows the equivalence theorem applied to replace the enclosed region with equivalent electric and magnetic surface currents ($\mathbf{J}_s$ and $\mathbf{M}_s$) on the NTFF surface. These equivalent currents are used to calculate far-field quantities while ensuring that the field solutions outside the NTFF surface remain unchanged. The dashed orange line represents the NTFF boundary, showcasing the region of integration in the NTFF formulation.

2.2. NTFF implementations for FDTD simulations

For the case of an FDTD simulation, there exists several methods to deal with the un-collocated nature of the calculated equivalent surface currents. In this paper, we follow the scheme proposed in [26,27] for the NTFF box selection. As depicted in Fig. 2(a-1), the calculated magnetic surface currents are aligned with the electric field, and thus no interpolation is needed, only a 1/2 factor is introduced as a weighting for elements that lie on the boundaries of the surfaces. As for the equivalent electric current calculations depicted in Fig. 2(a-2), an averaging process is utilized to take account for the 2 adjacent magnetic fields.

The averaging process could be arithmetic or geometric. It has been shown in [27] that taking the geometric mean gives better results than the arithmetic mean. In [28], a comparative study is provided in detail. The FDTD numerical examples shown in this paper utilize the NTFF scheme

Optics EXPRESS

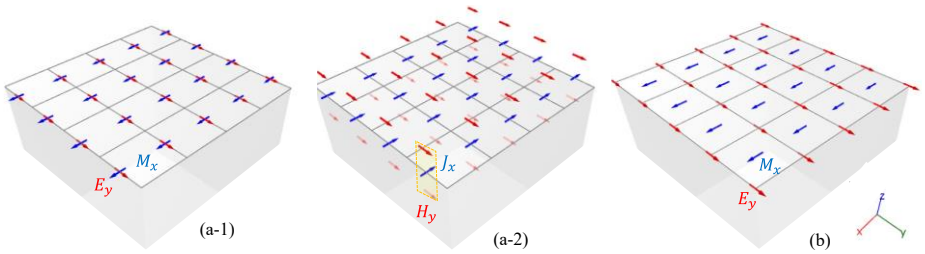

Fig. 2. NTFF transformation scheme for (a) FDTD and (b) PSTD simulations, showing the top surface with the x-component of the equivalent surface currents. (a-1) illustrates the calculation of magnetic currents in FDTD, aligned with the electric field, while (a-2) shows the calculation of electric currents using adjacent magnetic fields. (b) depicts the PSTD case, where collocated electric and magnetic fields allow the calculation of surface currents via the proposed sinc interpolation method.

shown in Fig. 2(a), and geometric mean is applied to average the magnetic field in order to correctly calculate the equivalent electric currents.

2.3. Proposed NTFF transformation for PSTD simulations

The difference between PSTD and FDTD mainly lies in their way of taking the spatial derivatives. For a Fourier-based PSTD scheme, the formulation yields a uniform collocated grid structure for field computations, and thus simplifies many cumbersome processes such as material or field averaging caused by the Yee grid structure in FDTD. Also, since PSTD capitalizes on the spectral characteristics of a function to approximate differentiation, which means that all the available field information is utilized to approximate partial derivatives, thereby nearing the Nyquist limit for recovering special field distributions with a sampling rate of at least two points per wavelength. This characteristic enables us to effectively capture the intricate temporal dynamics embedded within the PSTD simulation despite the limitations imposed by its grid resolution.

Considering the NTFF scheme shown in Fig. 2(b), since the electric and magnetic fields are collocated, the calculations of the magnetic and electric surface currents share the same spatial configuration. In our proposed scheme, the equivalent surface currents are equally spaced in between the fields, and each of them occupies the same size of area; thus, no weighting is needed as illustrated in the FDTD case. Instead of taking arithmetic or geometric mean to perform the calculation of the fictitious currents, it is the task of this paper to utilize the advantages of PSTD to accurately evaluate the equivalent surface currents from all the computed field values located at the same NTFF plane via a modified sinc interpolation. It had been shown in [29] that by exploiting the information embedded within a coarse grid via sinc interpolation, the correct field values can be theoretically reconstructed, and is far more accurate than any other numerical mean method.

We confine our discussion in 1D representation of the interpolation scheme for simplicity. The formulation for the 2D case (i.e. the six imaginary planes on the NTFF box) can be easily derived. As proposed in [29], the field information inside the simulation space can be perfectly recovered by interpolation of the field values with the sinc function

$$f(\eta) = \frac{\sin(2\pi W\eta)}{2\pi W\eta} = \frac{\sin(\pi\eta/\Delta\eta)}{\pi\eta/\Delta\eta} = \mathrm{sinc}(\eta/\Delta\eta), \quad \eta := x, y, z \tag{4}$$

where $W = N/2L$ is the approximated bandwidth in the spatial domain, N is the total number of field points in η direction, and $L = N\Delta\eta$ is the total extend of the simulation space in η direction. Theoretically, any field in between can be acquired by the infinite sum if Nyquist limit is followed

Optics EXPRESS

for the sampling of the field distribution

$$\psi(\eta) = \sum_{n=-\infty}^{\infty} \psi_n f(\eta - n\Delta\eta) = \sum_{n=-\infty}^{\infty} \psi_n \frac{\sin(\pi(\eta/\Delta\eta - n))}{\pi(\eta/\Delta\eta - n)} \tag{5}$$

where $\psi_n = \psi(n\Delta\eta)$ represents the field samplings, i.e., the calculated field values from PSTD simulations. However, this scheme may be unrealizable due to the finite length of the simulation space. This may impose little accuracy issue if the boundary field values taken account lies in the perfectly matched layers (PMLs). For cases where only a portion of the simulation space is considered, like the situation when we are to calculate the equivalent surface currents from the field values on a finite NTFF plane, there is a need to modify the representation in (5) to accommodate the situation.

In [30], a modification of sinc interpolation for the periodic finite case is derived from previous works [31,32]

$$\begin{aligned} \psi(\eta) &= \textstyle\sum_{n=N_l}^{N_u} \psi_n g(\eta - n\Delta\eta) \ , \\ g(\eta) &= \begin{cases} \frac{\sin(\pi\eta/\Delta\eta)}{N\sin(\pi\eta/N\Delta\eta)} \ , & N \ odd \\ \frac{\sin(\pi\eta/\Delta\eta)}{N\tan(\pi\eta/N\Delta\eta)} \ , & N \ even \end{cases} \end{aligned} \tag{6}$$

with $N_u - N_l = N$ being the period of the signal. This representation gives accurate results if the samplings are taken over a period, otherwise the interpolation process still suffers from signal oscillations at the boundaries of the interpolated data [33]. A simple method which does not alter the main formulation but still yields faithful interpolation results is to apply a well-chosen smooth low pass filter in the convolution process

$$\psi(\eta) = \sum_{n=-N_l}^{N_u} \psi_n g(\eta - n\Delta\eta)\mathrm{sinc}^2((\eta - n\Delta\eta)/2\Delta\eta) \tag{7}$$

In (7), a broadened squared sinc function is chosen as a multiplication factor to the applied kernel. It had been tested by the authors that when applying the filtering in (7), both kernels (sinc or the modified) give nearly the same results for interpolation. However, we still use the modified kernel $g(\eta)$ for implementation. To apply this method to the NTFF transformation, the formulation is extended to a double summation formulation, and ψ in (7) is replaced by the Cartesian components of the electric field $\mathbf{E}$ and magnetic field $\mathbf{H}$. Instead of interpolating at an arbitrary position, the equivalent surface currents are calculated at the center of the rectangular patch formed by four adjacent grid nodes. This approach ensures that each surface current occupies an equal area, eliminating the need for weight factors. By leveraging the interpolation method in this manner, the NTFF transformation is more effectively applied to the PSTD simulation.

Although not the primary aim of this paper, an extension to the staggered Fourier PSTD can also be considered. For staggered Fourier PSTD NTFF transformations, while it is feasible to directly apply various Yee-grid FDTD formulations, the proposed method can still be employed with slight modifications. It is noted that we can choose the positions of the fictitious currents in the staggered case to be the same as in the collocated case. For the calculation of surface magnetic currents, a 1D interpolation is utilized along the direction where the electric fields are at the boundaries and is repeated along the other direction. For the surface electric currents, the geometric means proposed in [27] can be used to calculate the fields aligned on the NTFF surface first, followed by the same repetitive 1D interpolation. This hybrid method reduces the use of the 1/2 factor commonly found in most FDTD NTFF transformation schemes while still benefiting from the spectral accuracy of PSTD calculations.

In short, despite the simulation being confined to discrete grid points, it is possible to interpolate field values at arbitrary spatial positions based on the coarse sample values. By leveraging

Optics EXPRESS

a generalized sinc function interpolation scheme, a high-resolution field distribution can be reconstructed. This approach unveils the intricate details of the field distribution that were obscured within the collocated PSTD grid, as opposed to the arithmetic or geometric mean used in FDTD, effectively enhancing the fidelity of the simulated results, and enabling a more accurate analysis of NTFF transformation.

3. Numerical results

In this section, we present the PSTD/FDTD simulation results for a simple dipole source radiation and homogeneous dielectric sphere scattering. These examples are chosen because analytic solutions exist for both cases, allowing for a comparison with the numerical results. To demonstrate the effectiveness of the NTFF calculation in the PSTD algorithm compared to FDTD, we use the same simulation settings for both algorithms as closely as possible, i.e., the same grid resolutions and time step, the same size of the simulation space, etc. Although using FDTD with a coarse grid may not be entirely fair due to its requirement for finer grid resolutions, we ensure that the simulation parameters, such as grid resolution and time steps, are as consistent as possible across both methods for comparison.

The NTFF computation for FDTD follows the second scheme proposed in subsection 2.2, utilizing the geometric mean for the calculation of the equivalent electric surface currents. The schematics of the numerical examples are shown in Fig. 3. The 3D PSTD/FDTD codes used in this paper are written in Julia. The grid representation of the sphere in Fig. 3(b) was generated using the VoxelModel package [34], and the radiation patterns were plotted with RadiationPatterns [35]. In the following simulations, a Gaussian pulse $g(t) = e^{-(t-t_0)^2/\tau^2}$ is used as the excitation waveform function with the parameters $\tau = \sqrt{2.3}/2\pi f_c, f_c$ equals to 600 THz, and $t_0 = 4.5\ \tau$.

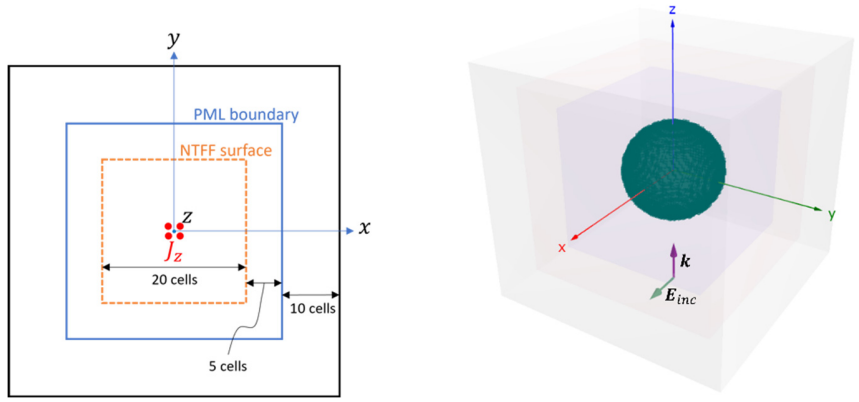

(a) (b)

Fig. 3. Schematics of the (a) dipole source radiation and (b) scattering from a dielectric sphere. In (a), the top-view schematic with detailed settings is shown. The sources are utilized in a twin-fashion to eliminate Gibbs phenomena. In (b), the full 3D schematic is provided. The grey boundary encloses the whole simulation space, inside it is the PML boundary (pink) and the NTFF surface (purple). The dielectric sphere is illuminated by a plane wave propagating in the $+z$-direction.

3.1. Dipole source radiation

Dipole source radiation has been the simplest case for testing the effectiveness of a NTFF transformation scheme, since its setting is simple, and the radiation solution is well-known.

Optics EXPRESS

For an infinitesimal electric current source placing along z-direction, the directivity pattern is 1.5 $\sin^2(\theta)$, and the directivity value is 1.5 [36], (section 4.2).

In this example, a J_z current source is placed at the center of the simulation space. In order to eliminate Gibbs phenomena caused by the field discontinuity, a twin-source scheme is applied, which occupies the 8 cells surrounding the origin [37]. The gird size is 0.05 μm (1/10 wavelength of 600 THz) in each direction. The simulation is composed of a $50 \times 50 \times 50$ cells grid, with 10-cell PML placing at the boundaries. The time step is 0.05 fs, and a total time of 25 fs (500 steps) is simulated. The NTFF surface is selected with a 5-cell distance apart from the PML, and a full 3D far-field pattern is calculated for a 1-degree precision in both θ- and ϕ-direction. The top-view schematic of the simulation setting is shown in Fig. 3(a). Served as a comparison, the FDTD modeling retains the same configuration and parameters as the PSTD simulation.

The calculated directivity results at 600 THz are shown in Fig. 4. In Fig. 4(a), the horizontal patterns in linear scale are presented. The result obtained by FDTD exhibits a ripple-like pattern, with a calculated directivity value of 1.5475. This discrepancy is likely due to the relatively coarse grid size, numerical anisotropy, and the 1/2 factor used in the NTFF scheme, all of which can introduce errors in the FDTD results. In contrast, the PSTD result shows agreement with the analytical solution, with a calculated directivity value of 1.5075. The 3D dipole directivity pattern calculated by the proposed PSTD case in dB scale is shown in Fig. 4(b). The light blue plane indicates the calculated 2D cut.

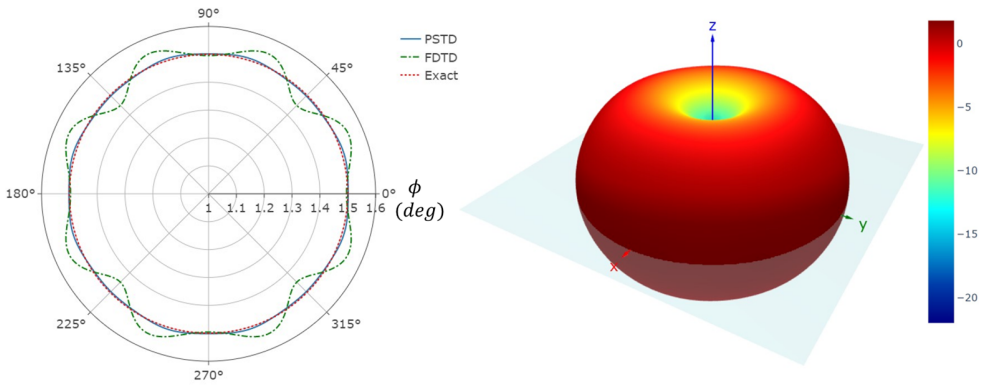

(a) (b)

Fig. 4. (a) The calculated horizontal cut of the directivity pattern in linear scale for PSTD, FDTD and the exact solution. (b) 3D directivity pattern for the PSTD case. The targeted wavelength is 600 THz, and the gird resolution in this simulation is 1/10 wavelength. One can observe an obvious ripple for FDTD results in the horizontal cut. The PSTD results, on the contrary, closely align with the analytic solution for both cuts. The calculated directivity is 1.5075 for PSTD and 1.5475 for FDTD, compared to the analytical value of 1.5.

3.2. *Scattering from a homogeneous dielectric sphere*

Since modeling dielectric sphere requires stair-cased approximation, there exists a higher requirement for grid resolution. For example, as the case demonstrated in [27], the radius of the sphere is discretized with 60 cells (with a cell size approximately equals to 1/20 wavelength). Another issue arises in FDTD while simulating nonuniform dielectric coefficient distribution over the space is the need to perform material averaging due to the Yee grid structure. In this example, we use the method in [26] to calculate the effective dielectric coefficients over the simulation space, where 4 surrounded values are used to take the arithmetic mean. For collocated PSTD, this averaging process is not needed since the field calculations are at the same positions for all

Optics EXPRESS

three directions. The analytic solution in this example is calculated with Mie theory, with which we make use of the MiePlot Software as our comparison [38].

In this simulation example, a homogeneous dielectric sphere with its relative dielectric coefficient $\epsilon_r = 2.25$ (refractive index $n = 1.5$) and radius equal to 0.5 μm (one wavelength at 600 THz) is simulated, with a discretization of 15 cells per wavelength for the simulation space in each direction. The simulation is composed of an $80 \times 80 \times 80$ cells grid, with 10-cell PML placing at the boundaries. The time step is 0.03 fs, and a total time of 60 fs (2000 steps) is simulated. The plane wave source is introduced into the space by pure scattered-field (SF) formulation, with its propagation towards $+z$-direction, and the electric field polarized along $+x$-direction (E_θ). The NTFF surface is selected with a 7-cell distance apart from the PML, and a full 3D radar cross section (RCS) pattern is calculated for a 1-degree precision in both θ- and ϕ-direction. The RCS is calculated by the following

$$RCS_\theta = \frac{k^2}{8\pi\eta_0 P_{inc}} |L_\phi + \eta_0 N_\theta|^2 \tag{8.a}$$

$$RCS_\phi = \frac{k^2}{8\pi\eta_0 P_{inc}} |L_\theta - \eta_0 N_\phi|^2 \tag{8.b}$$

where $k = 2\pi/\lambda$ and $P_{inc} = |E_{inc}(\omega)|^2/2\eta_0$, with $E_{inc}(\omega)$ being the DFT of the incident electric field waveform at the calculated frequency. The schematic of the simulation model is shown in Fig. 4(b). The calculated RCS_θ for $\phi = 0°$ cut and the 3D total radar cross section pattern in dB scale at 600 THz are shown in Fig. 5(a) and 5(b), respectively.

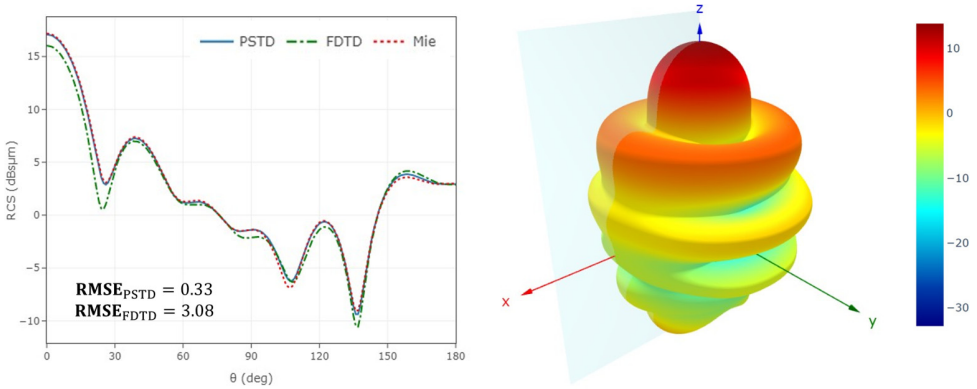

(a) (b)

Fig. 5. RCS analysis of scattering from a dielectric sphere with a diameter of 1 μm. The targeted frequency of this simulation is 600 THz, and the grid resolution is 1/15 wavelength. The refractive index of the sphere is 1.5. The (a) RCS_θ pattern for $\phi = 0°$ cut in dB scale for PSTD, FDTD and the analytical solution calculated by MiePlot and (b) the 3D total radiation cross section pattern calculated by the proposed method are shown. The RCS results are shown in the unit of dB squared μm. One can note that results obtained by PSTD align closely with the analytical solutions, while results obtained by FDTD exhibit certain deviations at the peaks and nulls of the pattern. The RMSE analysis demonstrates that the PSTD NTFF method achieves an accuracy that is an order of magnitude higher than the FDTD NTFF method.

One can see from Fig. 5(a) that with such resolution used for this simulation (1/15 wavelength per grid, modelling a 1-wavelength radius dielectric sphere), results obtained from PSTD still agree with the results calculated by Mie theory. As for FDTD, the computed values exhibit non-negligible deviations from the analytic solutions in the forward-scattering direction and the

Optics EXPRESS

nulls of the scattering pattern. The root-mean-square error (RMSE) compared with the Mie result (in linear scale) for both PSTD and FDTD are calculated: the RMSE of PSTD is 0.33, and the RMSE of FDTD is 3.08. The RMSE in FDTD is nearly an order of magnitude higher than in PSTD.

The simulation example is also carried out to compare the front ($\theta = 0°$) and back ($\theta = 180°$) RCS_θ at various wavelengths, which are shown in Fig. 6(a) and Fig. 6(b) respectively. The calculated wavelength ranges from 400 nm to 800 nm, with a 1 nm step. In this simulation, which requires a frequency span, we still use a constant relative dielectric coefficient for our sphere model. The previously shown simulation result corresponds to a wavelength of approximately 500 nm. As shown in Fig. 6, the PSTD results generally exhibit better agreement with the analytic results calculated using Mie theory compared to FDTD. A closer examination for Fig. 6(a) reveals that at shorter wavelengths (higher frequencies), the FDTD results show more deviations from the Mie results at the peaks and troughs of the spectral pattern as compared with PSTD results.

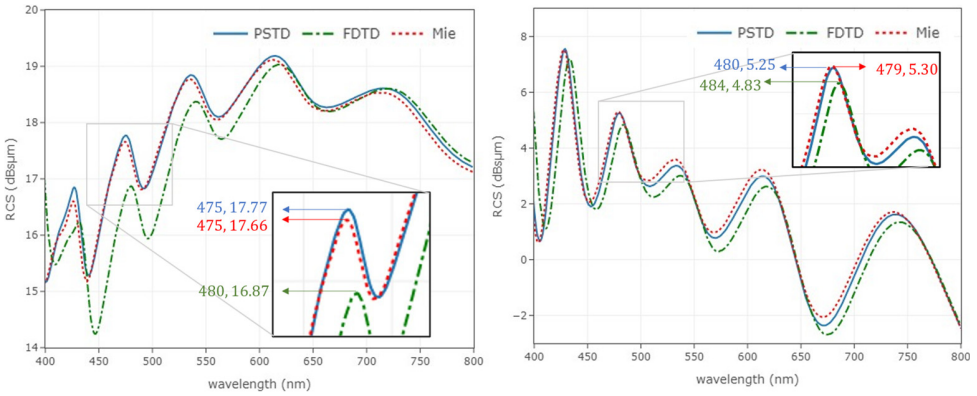

Fig. 6. The front and back scattered RCS values are analyzed across various wavelengths, building upon the previous simulation, using a fixed grid size of 1/30 μm. The (a) front ($\theta = 0°$) and (b) back ($\theta = 180°$) RCS in dB scale as a function of wavelength for PSTD, FDTD and the analytical solution calculated by MiePlot are shown. The wavelength ranges from 400 nm to 800 nm, with a 1 nm step. The results from the PSTD simulations maintain strong agreement with the Mie theory across the entire wavelength range. FDTD, on the other hand, shows deviations, particularly near the peaks and nulls of the RCS pattern, which become pronounced at specific wavelengths (e.g., 480 nm in the front-scattering case and 484 nm in the back-scattering case). The proposed PSTD NTFF method effectively demonstrates its capability in analyzing the Mie scattering problem across a broad wavelength range, even with a coarse grid.

Since the spectral patterns produced by the FDTD method exhibit noticeable shifts when compared to the Mie theory results, analyzing the RMSE becomes less insightful. Instead, we focus on examining the local maxima near the 500 nm region to assess the accuracy of the simulation methods in capturing the key scattering characteristics. For the front-scattered spectral pattern, the local maxima for Mie, PSTD and FDTD are 17.66 dBμsm at 475 nm, 17.77 dBμsm at 475 nm and 16.87 dBμsm at 480 nm, respectively; For the back-scattered spectral pattern, the local maxima for Mie, PSTD and FDTD are 5.30 dBμsm at 479 nm, 5.25 dBμsm at 480 nm and 4.83 dBμsm at 484 nm, respectively. The local maxima near 500 nm for PSTD differ by only 0.11 dBμsm in the front-scattered pattern and 0.05 dBμsm in the back-scattered pattern, while the wavelengths of the maxima coincide almost exactly with those of Mie theory (only 1 nm difference in the back-scattered case). On the other hand, The FDTD results show a clear shift in the wavelength at which the maxima occur, with a 5 nm shift in the front-scattered pattern and a

Optics EXPRESS

5 nm shift in the back-scattered pattern. Additionally, the FDTD spectral peaks are noticeably lower than both Mie and PSTD, with a 0.79 dBμsm difference in the front-scattered pattern and a 0.47 dBμsm difference in the back-scattered pattern. These discrepancies reflect limitations of FDTD in accurately capturing the spectral characteristics at these wavelengths.

4. Conclusion

In this paper, we introduced a NTFF transformation scheme optimized for PSTD simulations. Unlike traditional FDTD methods that rely on local averaging techniques (e.g., arithmetic or geometric means), which yield coarse approximations of the true value, our PSTD-based approach uses a modified sinc interpolation method. This method, based on the Nyquist theorem, offers a more accurate representation of the field values. By leveraging the proposed sinc interpolation, we achieve precise field recovery without the need for artificial smoothing or averaging processes. The numerical results for dipole source radiation and dielectric sphere scattering demonstrate the effectiveness of the proposed NTFF scheme in PSTD simulations. The PSTD method consistently provides results that closely match analytical solutions, even with coarse grid resolutions, whereas FDTD simulations exhibit significant deviations. This work underscores the potential of the proposed NTFF transformation scheme to enhance the accuracy of far-field calculations using the PSTD method and sets the stage for our future work in analyzing complex scattering problems in electromagnetic simulations.

Funding. National Science and Technology Council (112-2221-E-002 -203).

Disclosures. The authors declare no conflicts of interest.

Data availability. Data underlying the results presented in this paper are not publicly available at this time but may be obtained from the authors upon reasonable request.

References

1. K. R. Umashankar and A. Taflove, "A novel method to analyze electromagnetic scattering of complex objects," IEEE Trans. Electromagn. Compat. **EMC-24**(4), 397–405 (1982).
2. A. Taflove and K. R. Umashankar, "Radar cross section of general three-dimensional scatterers," IEEE Trans. Electromagn. Compat. **EMC-25**(4), 433–440 (1983).
3. A. Taflove, K. R. Umashankar, and T. G. Jurgens, "Validation of FD-TD modeling of the radar cross section of three-dimensional structures spanning up to nine wavelengths," IEEE Trans. Antennas Propag. **33**(6), 662–666 (1985).
4. R. J. Luebbers, K. S. Kunz, M. Schneider, *et al.*, "A finite-difference time-domain near zone to far zone transformation," IEEE Trans. Antennas Propag. **39**(4), 429–433 (1991).
5. K. S. Yee, D. Ingham, and K. Shlager, "Time-domain extrapolation to the far field based on FDTD calculations," IEEE Trans. Antennas Propag. **39**(3), 410–413 (1991).
6. K. Demarest, Z. Huang, and R. Plumb, "An FDTD near- to far-zone transformation for scatterers buried in stratified grounds," IEEE Trans. Antennas Propag. **44**(8), 1150–1157 (1996).
7. O. M. Ramahi, "Near- and far-field calculations in FDTD simulations using Kirchhoff surface integral representation," IEEE Trans. Antennas Propag. **45**(5), 753–759 (1997).
8. M. J. Barth, R. R. McLeod, and R. W. Ziolkowski, "A near- and farfield projection algorithm for finite-difference time-domain codes," J. Electromagn. Waves Applicat. **6**(1-4), 5–18 (1992).
9. T. Martin, "An improved near-to far-zone transformation for the finite-difference time-domain method," IEEE Trans. Antennas Propag. **46**(9), 1263–1271 (1998).
10. P.-W. Zhai, Y.-K. Lee, G. W. Kattawar, *et al.*, "Implementing the near- to far-field transformation in the finite-difference time-domain method," Appl. Opt. **43**(18), 3738–3746 (2004).
11. Y. Zeng and J. V. Moloney, "Polarization-current-based, finite-difference time-domain, near-to-far-field transformation," Opt. Lett. **34**(10), 1600–1602 (2009).
12. İ. R. Capoglu, A. Taflove, and V. Backman, "A frequency-domain near-field-to-far-field transform for planar layered media," IEEE Trans. Antennas Propag. **60**(4), 1878–1885 (2012).
13. T. Martin, "On the FDTD near-to-far-field transformations for weakly scattering objects," IEEE Trans. Antennas Propag. **58**(8), 2794–2795 (2010).
14. A. Ivanov, I. Valuev, S. Khilkov, *et al.*, *Fast computation of electromagnetic field in the far field zone based on spherical coordinates splitting*, (Springer International Publishing, Cham, 2021), pp. 73–86.
15. Q. H. Liu, "The PSTD algorithm: A time-domain method requiring only two cells per wavelength," Microw. Opt. Technol. Lett. **15**(3), 158–165 (1997).

Optics EXPRESS

16. Q. H. Liu, "Large-scale simulations of electromagnetic and acoustic measurements using the pseudospectral time-domain (PSTD) algorithm," IEEE Trans. Geosci. Remote. Sens. **37**(2), 917–926 (1999).
17. Q. H. Liu and G. Zhao, "Review of PSTD methods for transient electromagnetics," Int J Numerical Modelling **17**, 299–323 (2004).
18. C. Liu, R. Lee Panetta, and P. Yang, "Application of the pseudo-spectral time domain method to compute particle single-scattering properties for size parameters up to 200," J. Quant. Spectrosc. Radiat. Transfer **113**(13), 1728–1740 (2012).
19. Q. Li, Y. Chen, and D. Ge, "Comparison study of the PSTD and FDTD methods for scattering analysis," Microw. Opt. Technol. Lett. **25**(3), 220–226 (2000).
20. Q. Li and Y. Chen, "Applications of the PSTD for scattering analysis," IEEE Trans. Antennas Propag. **50**(9), 1317–1319 (2002).
21. S. H. Tseng, A. Taflove, D. Maitland, *et al.*, "Pseudospectral time domain simulations of multiple light scattering in three-dimensional macroscopic random media," Radio Sci. **41**(4), 1–5 (2006).
22. G. Chen, P. Yang, and G. W. Kattawar, "Application of the pseudospectral time-domain method to the scattering of light by nonspherical particles," J. Opt. Soc. Am. A **25**(3), 785–790 (2008).
23. R. L. Panetta, C. Liu, P. Yang, *et al.*, eds. (Heidelberg: Springer Berlin, 2013), pp. 139–188.
24. Y. Lei, M. S. Haynes, D. Arumugam, *et al.*, "A 2-D pseudospectral time-domain (PSTD) simulator for large-scale electromagnetic scattering and radar sounding applications," IEEE Trans. Geosci. Remote Sensing **58**(6), 4076–4098 (2020).
25. S. A. Schelkunoff, "Some equivalence theorems of electromagnetics and their application to radiation problems," The Bell Syst. Tech. J. **15**(1), 92–112 (1936).
26. S. Gedney, "Introduction to the Finite-Difference Time-Domain (FDTD) Method for Electromagnetics," Synthesis Lectures on Computational Electromagnetics **6**, 1 (2011).
27. D. J. Robinson and J. B. Schneider, "On the use of the geometric mean in FDTD near-to-far-field transformations," IEEE Trans. Antennas Propag. **55**(11), 3204–3211 (2007).
28. C. B. Ravi, F. H. Mohammed, J. P.-M. Melinda, *et al.*, "Near-to-far field transformation in FDTD: A comparative study of different interpolation approaches," The Applied Computational Electromagnetics Society Journal (ACES) **36**, 496–504 (2021).
29. J. W. Liu, Y. S. Hsu, and S. H. Tseng, "Extracting field information embedded within a coarse pseudospectral time-domain simulation," Antennas Wirel. Propag. Lett. **17**(8), 1488–1491 (2018).
30. S. R. Dooley and A. K. Nandi, "Notes on the interpolation of discrete periodic signals using sinc function related approaches," IEEE Trans. Signal Process. **48**(4), 1201–1203 (2000).
31. T. Schanze, "Sinc interpolation of discrete periodic signals," IEEE Trans. Signal Process. **43**(6), 1502–1503 (1995).
32. T. J. Cavicchi, "DFT time-domain interpolation," in *IEE Proceedings F* (1992), pp. 207–211.
33. L. Yaroslavsky, "Boundary effect free and adaptive discrete signal sinc-interpolation algorithms for signal and image resampling," Appl. Opt. **42**(20), 4166–4175 (2003).
34. J. W. Liu, "VoxelModel.jl," https://github.com/jake-w-liu/VoxelModel.jl (2024).
35. J. W. Liu, "RadiationPatterns.jl," https://github.com/jake-w-liu/RadiationPatterns.jl (2024).
36. A. Balanis, *Antenna Theory: Analysis and Design* (Wiley, 2016).
37. T.-W. Lee and S. C. Hagness, "A compact wave source condition for the pseudospectral time-domain method," Antennas Wirel. Propag. Lett. **3**, 253–256 (2004).
38. P. Laven, "MiePlot v4.6," http://www.philiplaven.com/mieplot.htm.